Solving Time-Dependent GinzburgLandau Equations in Comsol

Bakhrom Oripov

2018-05-01

1 Ginzburg-Landau theory

1.1 Free Energy

In 1950, 7 years before the BCS Theory, Ginzburg and Landau postulated the complete fundamental equations for macroscopic superconductivity. Their work is praised as the triumph of physical intuition. London equations, Abrikosov vortex lattice and Josephson relations, all can be derived from there. The GL free energy is the macroscopic elastic theory appropriate for any superconductor. The parameters for this free energy are the complex-valued "order parameter" $\Psi(\vec{r})$ and the vector potential $\vec{A}(\vec{r})$. The order parameter is what defines the superconducting state. If we separate the magnitude and the phase of $\Psi(\vec{r})$:

$$\Psi(\vec{r}) = |\Psi(\vec{r})|e^{i\theta(\vec{r})} \tag{1}$$

$$|\Psi(\vec{r})|^2 = n_s(\vec{r}) \tag{2}$$

where $n_s(\vec{r})$ is the superfluid density. The Ginzburg-Landau model defines superconductor as a charged Bose superfluid with particles of mass m_* and charge e_*.If superconducting state is fully destroyed in any domain within the sample of study, $n_s(\vec{r}) = 0$ there.

The total Ginzburg-Landau free energy has the form:

$$F_{tot}(\Psi(\vec{r}), \vec{A}(\vec{r})) = \int d^3\vec{r} F_{GL}(\vec{r}) \tag{3}$$

where the Ginzburg-Landau free energy density at the given position is:

$$F_{GL}(\vec{r}) = F_L(\Psi(\vec{r})) + F_{grad}(\Psi(\vec{r}), \vec{A}(\vec{r})) + U_{mag}(\vec{A}(\vec{r})) \tag{4}$$

Here F_L is Landau term which is the same free energy density as in the Landau mean field theory. It depends only on $\Psi(\vec{r})$ and doesn't include any direct effects that external magnetic field might have. Thus, it is the free energy density in a spatially uniform state and absence of external magnetic field. Assuming that F_L is an analytic function of $\Psi(\vec{r})$ we get

$$F_L(\Psi) = \alpha\Psi^2 + \frac{\beta}{2}\Psi^4 + ... \tag{5}$$

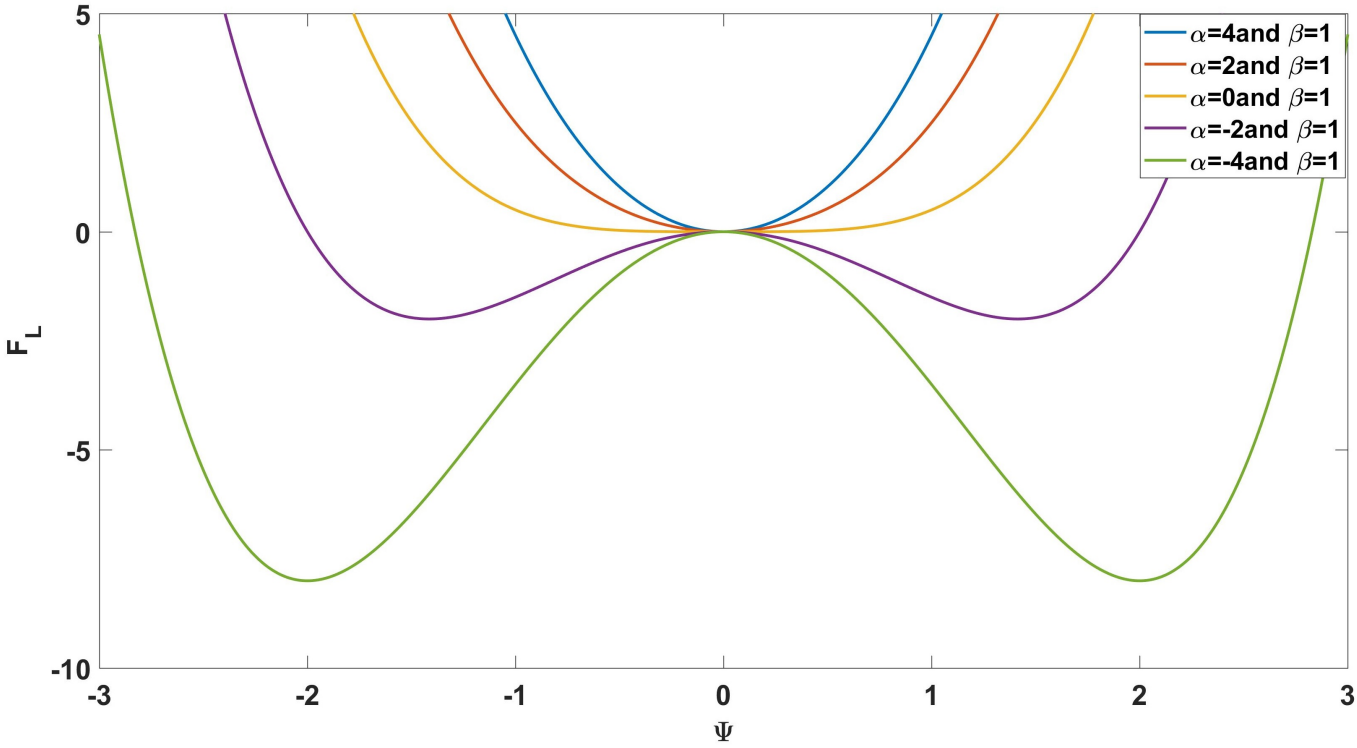

Figure 1: F_L vs Ψ for several α and β values.

Figure 1 shows the F_L vs Ψ for several α and β values. Here we see that for $\alpha > 0$ the minima for F_L occurs at $\Psi = 0$. This means that for any $\alpha > 0$ the ground state is the state with no superfluid density, thus normal state. For $\alpha < 0$ the minima for F_L occurs at $\Psi = \Psi_\infty$ where

$$\Psi_\infty = \sqrt{\frac{-\alpha(0)}{\beta}} \tag{6}$$

Since we expect a transition from superconductor state to normal state at the superconducting critical temperature T_c we know that α should go from negative to positive at T_c. And we also expect α to be an analytic function of temperature, so we can write:

$$\alpha(T) = \alpha^{'}(T - T_c) \tag{7}$$

The F_{grad} is a kinetic energy term and given by:

$$F_{grad}(\Psi, \vec{A}) = \frac{\hbar^2}{2m_*}|(\vec{\nabla} - \frac{ie_*}{\hbar}\vec{A})\Psi)|^2 \tag{8}$$

In a way its energy due to interaction of superconducting current and magnetic field.

Finally, $U_{mag}(\vec{A})$ is just the energy due to the magnetic field and given by the simple equation:

$$U_{mag}(\vec{A}) = \frac{1}{2\mu_0}|\vec{\nabla} \times \vec{A}|^2 \tag{9}$$

The detailed justification and derivation can be found in the lecture notes by Christopher L. Henley [1] and Phillip M. Duxbury [2]

Although the Ginzburg-Landau theory precedes the BCS theory, in 1959, Gorkov was able to derive the same equation from BCS theory in the limit where temperature is close to the superconducting critical temperature [3]. He showed that $\Psi \propto \Delta$ where Δ is the superconducting gap.

1.2 Time Dependence

If we rewrite (3) using (1) to substitute for both Ψ and Ψ^* we will end up with $F_{tot}(n_s, \theta)$. Since the phase θ and the superfluid charge density n_s are canonically conjugate we get Hamilton's equations of motion:

$$\hbar\frac{d\theta(\vec{r}, t)}{dt} = -\frac{\partial F_{tot}}{\partial n_s(\vec{r}, t)} \tag{10}$$

$$\hbar\frac{dn_s(\vec{r}, t)}{dt} = -\frac{\partial F_{tot}}{\partial \theta(\vec{r}, t)} \tag{11}$$

This leads to 2 Time-Dependent Ginzburg-Landau equations:

$$\frac{\hbar^2}{2m_* D}\frac{\partial \Psi}{\partial t} = -\frac{1}{2m_*}\left(\frac{\hbar}{i}\vec{\nabla} - e_*\vec{A}\right)^2 \Psi + \alpha\Psi - \beta|\Psi|^2\Psi \tag{12}$$

$$\sigma\frac{\partial \vec{A}}{\partial t} = \frac{e_*\hbar}{2m_* i}\left(\Psi^*\vec{\nabla}\Psi - \Psi\vec{\nabla}\Psi^*\right) - \frac{e_*^2}{m_*}|\Psi|^2\vec{A} - \frac{1}{\mu_0}\vec{\nabla} \times \vec{\nabla} \times \vec{A} \tag{13}$$

where $m_* = 2m_e$ is the mass of the Cooper pair, $e_* = 2e$ is the charge of the Cooper pair, D is the phenomenological diffusion coefficient and σ is the conductivity of the normal (non-superconducting) current.

Here the superconducting current can be obtained from the expectation value of the momentum operator:

$$\vec{J_s} = \frac{e_*\hbar}{2m_* i}\left(\Psi^*\vec{\nabla}\Psi - \Psi\vec{\nabla}\Psi^*\right) - \frac{e_*^2}{m_*}|\Psi|^2\vec{A} \tag{14}$$

1.3 Gauge Choice

Vinokur has a different set of TDGL equations in his paper [4] where the scalar electric potential Φ is also used:

$$\frac{\hbar^2}{2m_* D}\left(\frac{\partial}{\partial t} + i\frac{e_*}{\hbar}\Phi\right)\Psi = -\frac{1}{2m_*}\left(\frac{\hbar}{i}\vec{\nabla} - e_*\vec{A}\right)^2\Psi + \alpha\Psi - \beta|\Psi|^2\Psi \tag{15}$$

$$\sigma\left(\frac{\partial\vec{A}}{\partial t} + \vec{\nabla}\Phi\right) = \frac{e_*\hbar}{2m_* i}\left(\Psi^*\vec{\nabla}\Psi - \Psi\vec{\nabla}\Psi^*\right) - \frac{e_*^2}{m_*}|\Psi|^2\vec{A} - \frac{1}{\mu_0}\vec{\nabla}\times\vec{\nabla}\times\vec{A} \tag{16}$$

However, we know that the Ginzburg-Landau equations are gauge invariant. For any given function $\chi(x, y, z, t)$:

$$\widetilde{\Psi} = \Psi e^{i\kappa\chi}; \quad \widetilde{A} = A + \nabla\chi; \quad \widetilde{\Phi} = \Phi - \frac{\partial\chi}{\partial t}$$

would also satisfy the equation. In order to simplify the equation and remove the scalar potential Φ one could set

$$\frac{\partial\chi}{\partial t} = \Phi \tag{17}$$

and equations 15 and 16 will simplify to 12 and 13.

1.4 Assumptions

> "A continuous symmetry like $\Psi(\vec{r}) = |\Psi(\vec{r})|e^{i\Delta\theta(\vec{r})}$ normally implies the existence of a gapless Goldstone mode" [1]

.

> "These dynamic equations are microscopically justified only for gap-less superconductors" [5],[6].

1.5 Normalization

Lets introduce some normalized quantities:

$\widetilde{\Psi} = \dfrac{\Psi}{\Psi_\infty}$ where $|\Psi_\infty|^2 = -\dfrac{\alpha(0)}{\beta}$ is the bulk superfluid density at zero temperature in the absence of external magnetic field.

$\widetilde{x} = \dfrac{x}{\lambda_0}$ thus $\widetilde{\nabla} = \lambda_0 \nabla$ where x represents length and $\lambda_0 = \kappa \dfrac{\hbar}{\sqrt{2m\alpha_0}}$ is the zero temperature GL penetration depth. Here $\kappa = \dfrac{\lambda_0}{\xi_0}$ where ξ_0 is the zero temperature GL coherence length.

$\widetilde{B} = \dfrac{B}{B_{c2}}$ where $B_{c2} = \dfrac{\Phi_0}{\xi_0^2}$.

$\vec{\widetilde{A}} = \dfrac{\lambda_0}{\kappa^2 \Phi_0} \vec{A}$ where Φ_0 is the magnetic flux quantum.

$\widetilde{J} = \dfrac{J}{J_c}$ where $J_c = \dfrac{\mu_0 \lambda_0^3}{\kappa^2 \Phi_0} = \dfrac{B_{c2}}{\mu_0 \lambda_0}$.

$\widetilde{t} = \dfrac{t}{\tau_0}$ where $\tau_0 = \mu_0 \lambda_0^2 \sigma_n$.

$\eta = \dfrac{\tau_{GL}}{\tau_0}$ where $\tau_{GL} = \dfrac{\xi_0^2}{D}$ and D here is the phenomenological diffusion coefficient given by $D = \dfrac{v_F l}{3}$ [7] with v_F being the Fermi velocity and l being the quasiparticle mean free path [8].

$\widetilde{\sigma} = \dfrac{\sigma}{\sigma_n}$, where σ_n is the normal state conductivity.

Rewriting 12 and 13 using newly introduced quantities we get:

$$\eta \frac{\partial \widetilde{\Psi}}{\partial \widetilde{t}} = -\left(\frac{i}{\kappa} \widetilde{\nabla} + \kappa \widetilde{A} \right)^2 \widetilde{\Psi} + \left(\epsilon - |\widetilde{\Psi}|^2 \right) \widetilde{\Psi}$$

$$\widetilde{\sigma} \frac{\partial \widetilde{A}}{\partial \widetilde{t}} = \frac{1}{2\kappa^2 i} \left(\widetilde{\Psi}^* \widetilde{\nabla} \widetilde{\Psi} - \widetilde{\Psi} \widetilde{\nabla} \widetilde{\Psi}^* \right) - |\widetilde{\Psi}|^2 \widetilde{A} - \widetilde{\nabla} \times \widetilde{\nabla} \times \widetilde{A}$$

$$\widetilde{J} = \frac{1}{2\kappa^2 i} \left(\widetilde{\Psi}^* \widetilde{\nabla} \widetilde{\Psi} - \widetilde{\Psi} \widetilde{\nabla} \widetilde{\Psi}^* \right) - |\widetilde{\Psi}|^2 \widetilde{A}$$

where $\epsilon(\vec{r}, T) = \dfrac{\alpha(\vec{r}, T)}{\alpha_\infty}$ and $\alpha_\infty = \alpha(Bulk, 0) = -\alpha' T_c$. Any localized defect, or nonzero temperature can be specified through ϵ.

2 TDGL for Comsol

2.1 Normalized TDGL and Boundary Conditions

In the previous section we derived the normalized TDGL Equations. Lets rewrite them by dropping superscripts:

$$\eta \frac{\partial \Psi}{\partial t} = -\left(\frac{i}{\kappa} \vec{\nabla} + \kappa \vec{A} \right)^2 \Psi + \left(\epsilon - |\Psi|^2 \right) \Psi \tag{18}$$

$$\sigma\frac{\partial\vec{A}}{\partial t}=\frac{1}{2\kappa^2 i}\left(\Psi^*\vec{\nabla}\Psi-\Psi\vec{\nabla}\Psi^*\right)-|\Psi|^2\vec{A}-\vec{\nabla}\times\vec{\nabla}\times\vec{A} \tag{19}$$

$$\vec{J}=\frac{1}{2\kappa^2 i}\left(\Psi^*\vec{\nabla}\Psi-\Psi\vec{\nabla}\Psi^*\right)-|\Psi|^2\vec{A} \tag{20}$$

From now on, all the equations will be written in normalized form referring to section 1.5 .

Now, we want to numerically simulate the superconducting domain, we need to specify the boundary conditions. Any current passing through the boundary between a superconducting domain and vacuum/insulator would be non-physical, thus we expect:

$$\vec{J}\cdot\hat{n}=0\quad on\quad \partial\Omega \tag{21}$$

Here $\hat{n}$ is unit vector normal to the boundary, and since we expect (21) to be true even when $\vec{A}=0$ and $\Psi\neq 0$ the first boundary condition is:

$$\vec{\nabla}\Psi\cdot\hat{n}=0\quad on\quad \partial\Omega \tag{22}$$

there should also be no normal state current through the boundary thus

$$\vec{E}\cdot\hat{n}=0 \tag{23}$$

and since $\vec{E}=-\dfrac{\partial\vec{A}}{\partial t}$

$$\frac{\partial\vec{A}}{\partial t}\cdot\hat{n}=0 \tag{24}$$

and by integrating we can write:

$$\vec{A}\cdot\hat{n}=0\quad on\quad \partial\Omega \tag{25}$$

The third boundary condition generally used is the continuity of magnetic field.

$$\vec{\nabla}\times\vec{A}=B_{external}\quad on\quad \partial\Omega \tag{26}$$

2.2 Rewriting for Comsol

Comsol can efficiently solve several types of mathematical equations, one of which is General Form Partial Differential Equation:

$$d_a\frac{\partial\vec{x}}{\partial t}+\vec{\nabla}\cdot\vec{\Gamma}=\vec{F} \tag{27}$$

where

$$d_a=\begin{bmatrix} d_{11} & d_{12} & ... & ... & d_{1m}\\ d_{21} & d_{22} & ... & ... & ...\\ ... & ... & ... & ... & ...\\ ... & ... & ... & ... & ...\\ d_{m1} & ... & ... & ... & d_{mm}\end{bmatrix}\quad \vec{x}=\begin{bmatrix} x_1\\ x_2\\ ...\\ ...\\ x_m\end{bmatrix}\quad \vec{\Gamma}=\begin{bmatrix} g_{11} & g_{12} & g_{13}\\ g_{21} & g_{22} & g_{23}\\ ... & ... & ...\\ ... & ... & ...\\ g_{m1} & g_{m2} & g_{m3}\end{bmatrix}\quad \vec{F}=\begin{bmatrix} f_1\\ f_2\\ ...\\ ...\\ f_m\end{bmatrix}$$

Now we need to rewrite 18 and 19 so that we can put it into this form. We will rewrite [9]:

$$\Psi = v_1 + iv_2 \tag{28}$$

$$\vec{A} = A_1\hat{x} + A_2\hat{y} + A_3\hat{z} \tag{29}$$

After some simple mathematical rearrangement we get an equation similar to 27:

$$\begin{bmatrix} \eta & 0 & 0 & 0 & 0 \\ 0 & \eta & 0 & 0 & 0 \\ 0 & 0 & \sigma & 0 & 0 \\ 0 & 0 & 0 & \sigma & 0 \\ 0 & 0 & 0 & 0 & \sigma \end{bmatrix} \cdot \frac{\partial}{\partial t} \begin{bmatrix} v_1 \\ v_2 \\ A_1 \\ A_2 \\ A_3 \end{bmatrix} + \begin{bmatrix} \frac{\partial}{\partial x} & \frac{\partial}{\partial y} & \frac{\partial}{\partial x} \end{bmatrix} \cdot \begin{bmatrix} -\frac{v_{1x}}{\kappa^2} & -\frac{v_{1y}}{\kappa^2} & -\frac{v_{1z}}{\kappa^2} \\ -\frac{v_{2x}}{\kappa^2} & -\frac{v_{2y}}{\kappa^2} & -\frac{v_{2z}}{\kappa^2} \\ 0 & A_{2x} - A_{1y} & A_{3x} - A_{1z} \\ A_{1y} - A_{2x} & 0 & A_{3y} - A_{2y} \\ A_{1z} - A_{3x} & A_{2z} - A_{3y} & 0 \end{bmatrix} = \vec{F} \tag{30}$$

$$\vec{F} = \begin{bmatrix} \frac{(A_{1x} + A_{2y} + A_{3z})}{\kappa} v_2 + \frac{2\left(A_1 v_{2x} + A_2 v_{2y} + A_3 v_{2z}\right)}{\kappa} - (A_1^2 + A_2^2 + A_3^2) v_1 + \left(\epsilon - \left(v_1^2 + v_2^2\right)\right) v_1 \\ -\frac{(A_{1x} + A_{2y} + A_{3z})}{\kappa} v_1 - \frac{2\left(A_1 v_{1x} + A_2 v_{1y} + A_3 v_{1z}\right)}{\kappa} - (A_1^2 + A_2^2 + A_3^2) v_2 + \left(\epsilon - \left(v_1^2 + v_2^2\right)\right) v_2 \\ \frac{(v_1 v_{2x} - v_2 v_{1x})}{\kappa^2} - \left(v_1^2 + v_2^2\right) A_1 \\ \frac{(v_1 v_{2y} - v_2 v_{1y})}{\kappa^2} - \left(v_1^2 + v_2^2\right) A_2 \\ \frac{(v_1 v_{2z} - v_2 v_{1z})}{\kappa^2} - \left(v_1^2 + v_2^2\right) A_3 \end{bmatrix} \tag{31}$$

with simple boundary conditions:

$$\vec{\nabla}\Gamma \cdot \hat{n} = 0 \quad on \quad \partial\Omega \tag{32}$$

$$\vec{A} \cdot \hat{n} = 0 \quad on \quad \partial\Omega \tag{33}$$

and

$$\vec{\nabla} \times \vec{A} = \vec{\nabla} \times \vec{A_{ext}} \quad on \quad \partial\Omega \tag{34}$$

Here v_{1x} means $\frac{\partial v_1}{\partial x}$ and so on...

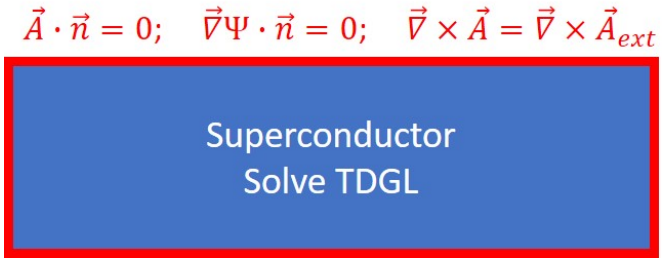

Figure 2: The superconducting domain and boundary conditions.

Eq 30 is solved in a superconducting domain with 32, 33 and 34 being the boundary conditions. This is represented in Figure 2.

2.3 Reproducing known results

We first tested the accuracy of our simulation by reproducing some published results. The example provided here is the result of the Danish group [9], where A 2-dimensional $10\lambda_0$ by $10\lambda_0$ rectangular domain was simulated in Comsol. A uniform external magnetic field is applied perpendicular to the surface of this 2D superconducting domain with $\kappa = 4$. The system is at 0K temperature and started from fully superconducting state at $t = 0$. Figure 3 shows the plot of Ψ^2 along with the comparison of our result with the original at $B = 0.1875$ and $t = 35$. All quantities normalized as described in section 1.5. Figure 4 has the result for same scenario at a later time, t=100;

We can clearly see how vortices penetrate through the boundary and come into equilibrium at the center.

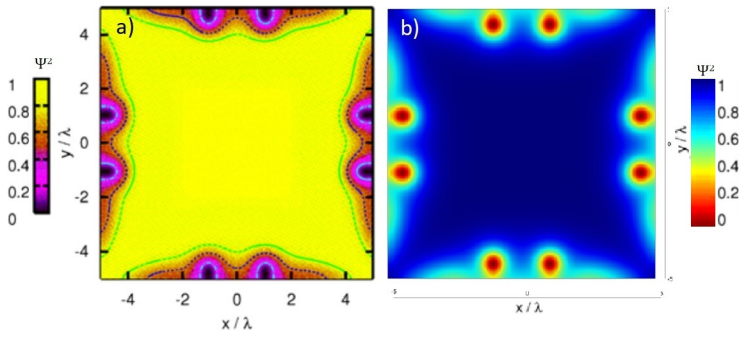

Figure 3: Ψ^2 plot at $t = 35$ and $B = 0.75/\kappa$ a) Result by Pedersen b) our result

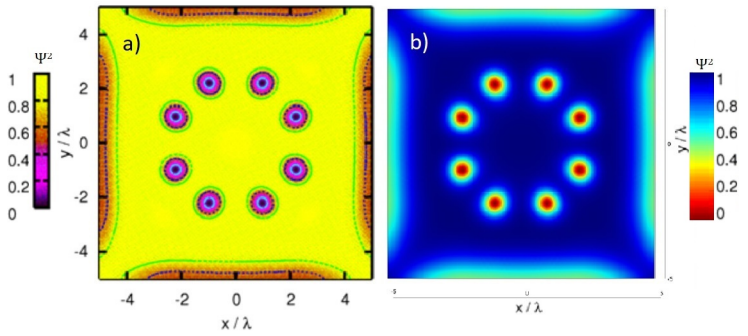

Figure 4: Ψ^2 plot at $t = 100$ and $B = 0.75/\kappa$ a) Result by Pedersen b) our result

2.3.1 Argument about Boundary condition: Superconducting Sphere inside uniform magnetic field

Many papers that we reviewed use 34 or 26 in SI units:

$$\vec{\nabla} \times \vec{A} = \vec{B}_{external} \quad on \quad \partial\Omega$$

However this implies that the superconducting screening current has no effect on magnetic field at the boundary and beyond the superconducting domain. This is physically wrong. The effect of screening currents is crucial when one is trying to simulate spatially nonuniform external magnetic field (like magnetic dipoles). We decided to use 2 domains for our calculations: Superconductor domain and Vacuum/Insulator surrounding it. We solve TDGL equations in the superconductor domain, and only solve Maxwell equations in the second domain. Equations 32 and 33 would still be valid at the superconductor/insulator boundary, however we will not use 34 there. Instead we enforce 34 at the outer boundary of our second domain where the contribution from the superconductor is negligible (assuming the second domain is big enough). Figure 5 shows this scenario in a schematic.

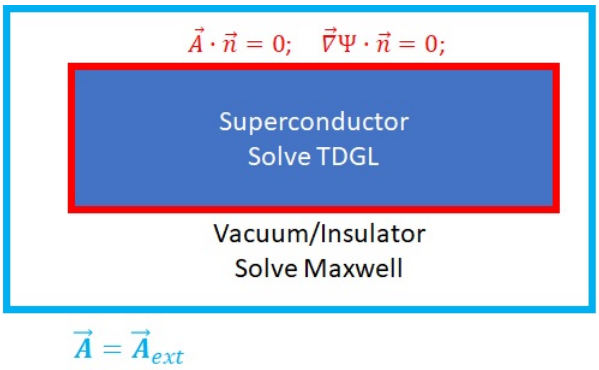

Figure 5: The 2 domains and boundary conditions.

To test our model we chose the simplest example: a superconducting sphere inside a uniform external magnetic field. We simulated the response of a superconducting sphere inside uniform magnetic field using our 2-domain method and conventional single domain method used by everyone else and later we compared both results with the analytic solution [10].

Figure 7 clearly shows that using the 2-domain model we can reproduce the exact analytic solution, while the single domain model fails to account for the enhancement of magnetic field on the surface of the sphere.

2.3.2 Point Magnetic Dipole: Separation of $\vec{A}$

The next step would be simulating the effect of spatially nonuniform magnetic field. Our magnetic writer probe can be approximated to the first degree to a point magnetic dipole. We want to ensure that we can accurately simulate the screening currents produced by the point magnetic dipole and compare to results obtained by Milosevich [11].

The superconducting domain and vacuum domain are simulated as 2 coaxial disks with equal radius R (see Figure 8. The height of the superconducting domain is H_{sc} and the height of the vacuum domain is H_{vac}. The point magnetic dipole is placed at a height H_{dipole} with magnetic moment $\vec{M}(t)$. In simulation, we don't specify $M(t)$ we rather specify the magnetic field produced at origin $\vec{B}(t)$ and the value for $\vec{M}(t)$ is chosen accordingly.

Minor issue here is the fact that at the location of the dipole $\vec{\nabla}\times\vec{\nabla}\times\vec{A}$ diverges, causing singularity in numerical simulation. The solution is to redefine $\vec{A}$ as follows:

$$\vec{A}=\vec{A}_{ext}+\vec{u} \tag{35}$$

where $\vec{A}$ is total vector potential, $\vec{u}$ contribution due to normal and superconducting currents in superconducting domain and $\vec{A}_{ext}$ is the externally applied vector potential (source located outside the superconducting domain).

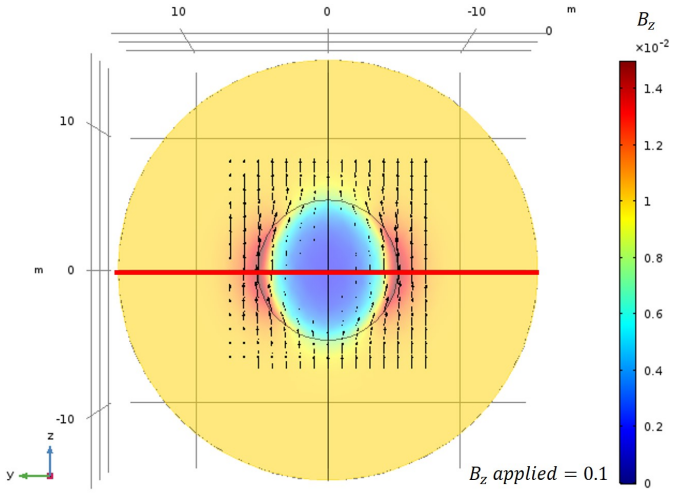

Figure 6: a superconducting sphere inside uniform magnetic field. sphere diameter is $10\lambda_0$; vacuum domain diameter is $30\lambda_0$ and $\kappa = 1$. Black arrows show vector magnetic field lines. Red line indicates the equator, the magnetic field along red line is shown in figure 7.

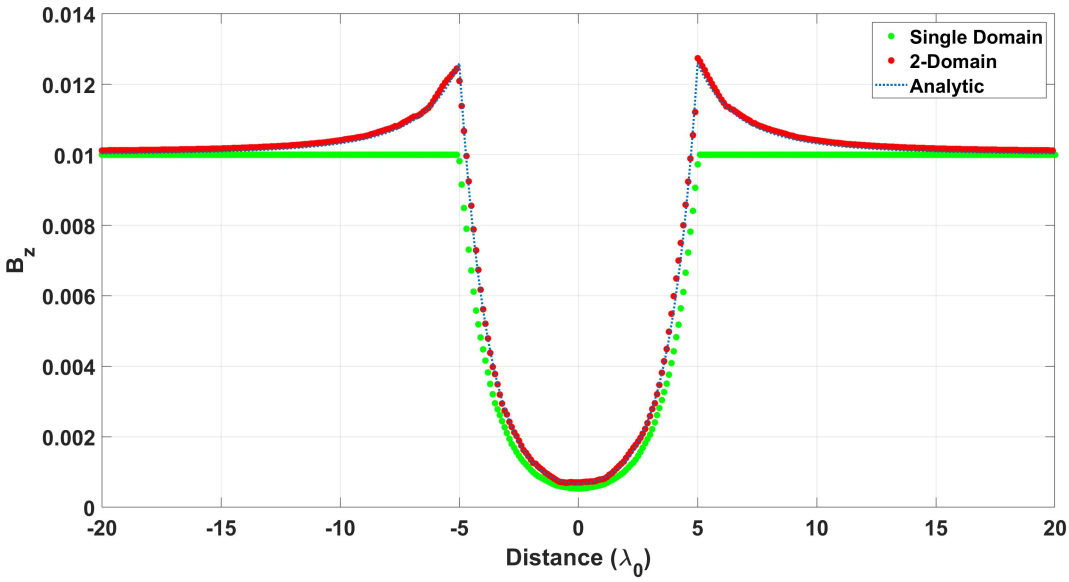

Figure 7: Magnetic field profile along the equator of sphere in Fig 6.

Once we redefine $\vec{A}$ as in Eq.(35) we do not solve for $\vec{A}$, we solve for $\vec{u}$ instead. Equation 30 has to be modified accordingly.

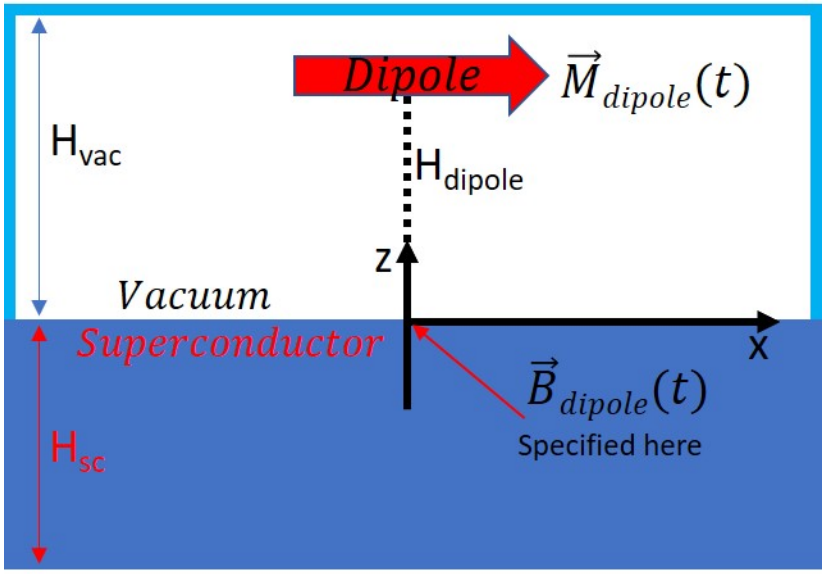

Figure 8: Diagram for the parallel point magnetic dipole above the superconductor

The following boundary conditions are enforced, assuming that both domains are sufficiently big enough and the effect of the point magnetic dipole vanishes at outer boundaries:

On the boundary between the superconducting domain and vacuum domain

$$\vec{\nabla}\Psi \cdot \hat{n} = 0 \quad or\ equally \quad \vec{\nabla}\Gamma \cdot \hat{n} = 0$$
$$and\ \vec{A} \cdot \hat{n} = 0 \quad or\ equally \quad \vec{u} \cdot \hat{n} = -\vec{A}_{ext} \cdot \hat{n}$$

On the boundary on top of vacuum domain

$$\vec{A} = \vec{A}_{ext} \quad or\ equally \quad \vec{u} = 0$$

On all other boundaries of the superconducting domain and vacuum domain

$$\vec{\nabla}\Psi \cdot \hat{n} = 0 \quad or\ equally \quad \vec{\nabla}\Gamma \cdot \hat{n} = 0$$
$$and\ \vec{A} = 0 \quad or\ equally \quad \vec{u} = -\vec{A}_{ext}$$

Figures 9 and 10 illustrate how similar our results are to the ones obtained by Milosevich. Figure 11 shows J_{surf} as function of distance from origin for the perpendicular dipole case (Figure 9). "TDGL" is the result we got from Comsol, "Analytic" is the result obtained by Milosevic [11] and "Numeric" is the result from numeric integration given by Melnikov [12]. Since Comsol is the numerical simulation, our result is more similar to the one obtained by Melnikov.

This way we verified that we can accurately simulate the response of the superconductor to externally applied spatially nonuniform magnetic field.

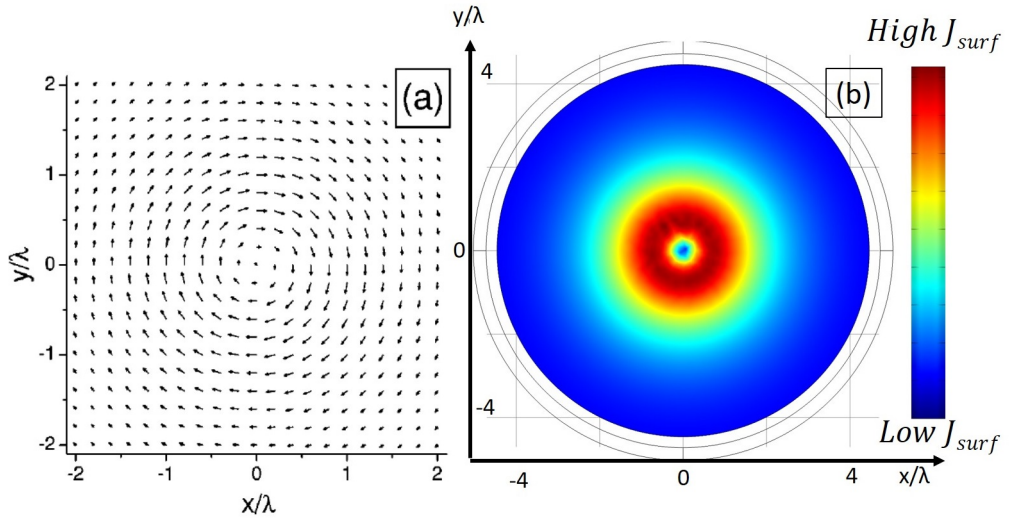

Figure 9: J_{surf} plot for perpendicular magnetic dipole at $H_{dipole} = 1$ a) Result by Milosevich b) our result

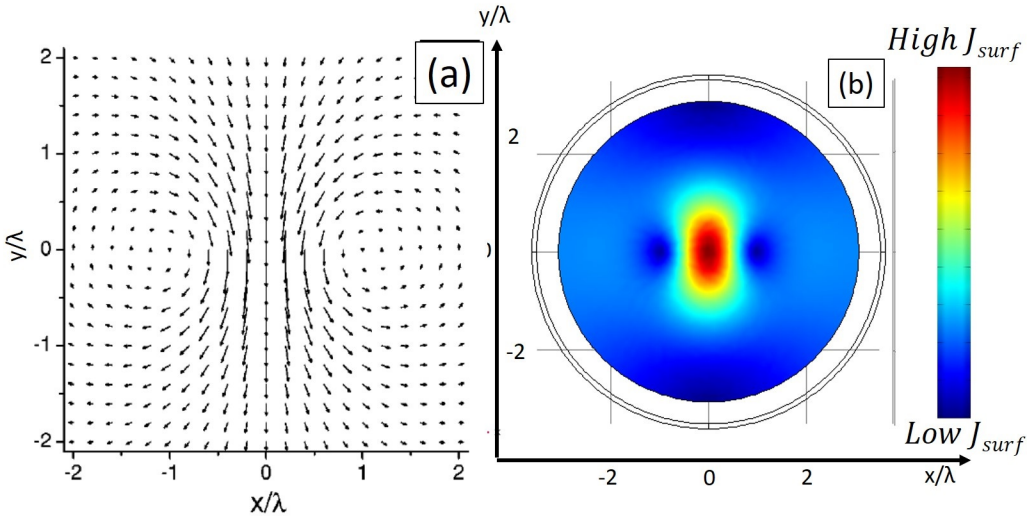

Figure 10: J_{surf} plot for parallel magnetic dipole at $H_{dipole} = 1$ a) Result by Milosevich b) our result

3 SRF Application

Gurevich and Ciovati had proposed a model to explain the dissipation produced by vortices in an SRF cavity [13]. Since SRF cavity is subjected to RF field, a vortex semiloop can penetrate into the bulk of the superconductor during the first half of the RF cycle, and an anti-vortex semi-loop can penetrate during the second half. For high values of peak RF magnetic field amplitude, vortex and anti-vortex semi-loops meet inside the superconductor snd annihilate

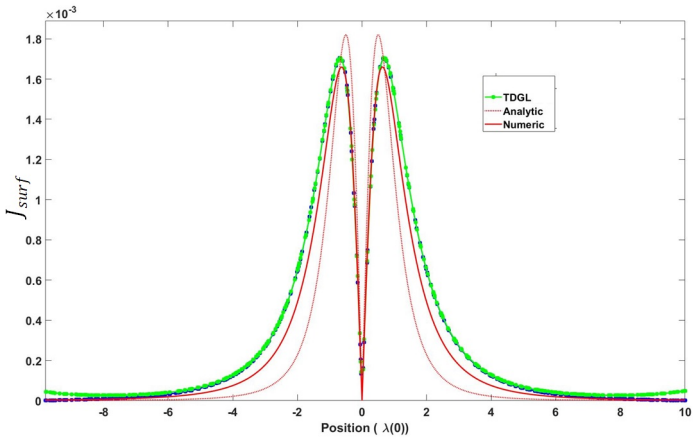

Figure 11: J_{surf} magnitude vs distance from origin.

each other. Quantitative calculation of dissipated power due to this mechanism was performed by Gurevich and Ciovati. The same idea was used by Tai to explain the harmonic response produced by Nb samples [14].

We will try to simulate this scenario in Comsol

3.1 TDGL Parameters for Nb

Before we start we need to gather relevant numbers for Nb from various sources:

σ_n ranges from $2 \times 10^8 S/m$ to $2 \times 10^9 S/m$ [15] depending on RRR value,

$\lambda_0 = 40nm$ [16] and $\kappa = 0.8$ [17]. Thus, $\tau_0 = \mu_0 \lambda_0^2 \sigma_n = 4\pi \times 10^{-7} H/m \times (40nm)^2 \times 2 \times 10^9 S/m = 4.02 \times 10^{-12} s$ for clean limit samples (RRR 300).

Period of $200\tau_0$ corresponds to $8.04 \times 10^{-10} s$ or experimental frequency of $f = 1.24GHz$. Considering that experiments are done at higher frequencies and also expanding this solution for dirty limit, Period can range from $100\tau_0$ to $2000\tau_0$.

$D = \frac{v_F \times l}{2} > \frac{1.37 \times 10^6 m/s \times 200nm}{2} = 0.137 m^2/s$[18] . Here 200nm is the optimal choice for quasiparticle mean free path, although other values are possible depending on Nb RRR value.

$$\tau_{GL} = \frac{\xi^2}{D} = \frac{\frac{\lambda_0^2}{\kappa^2}}{D} = 1.825 \times 10^{-14} s$$

$$\eta = \frac{\tau_{GL}}{\tau_0} \approx 4.54 \times 10^{-3}$$

3.2 Vortex Semiloops due to Magnetic Probe

The general scenario was explained in Section 2.3.2. Here we will just summarize our findings.

3.2.1 Time Evolution of Vortex Semiloop

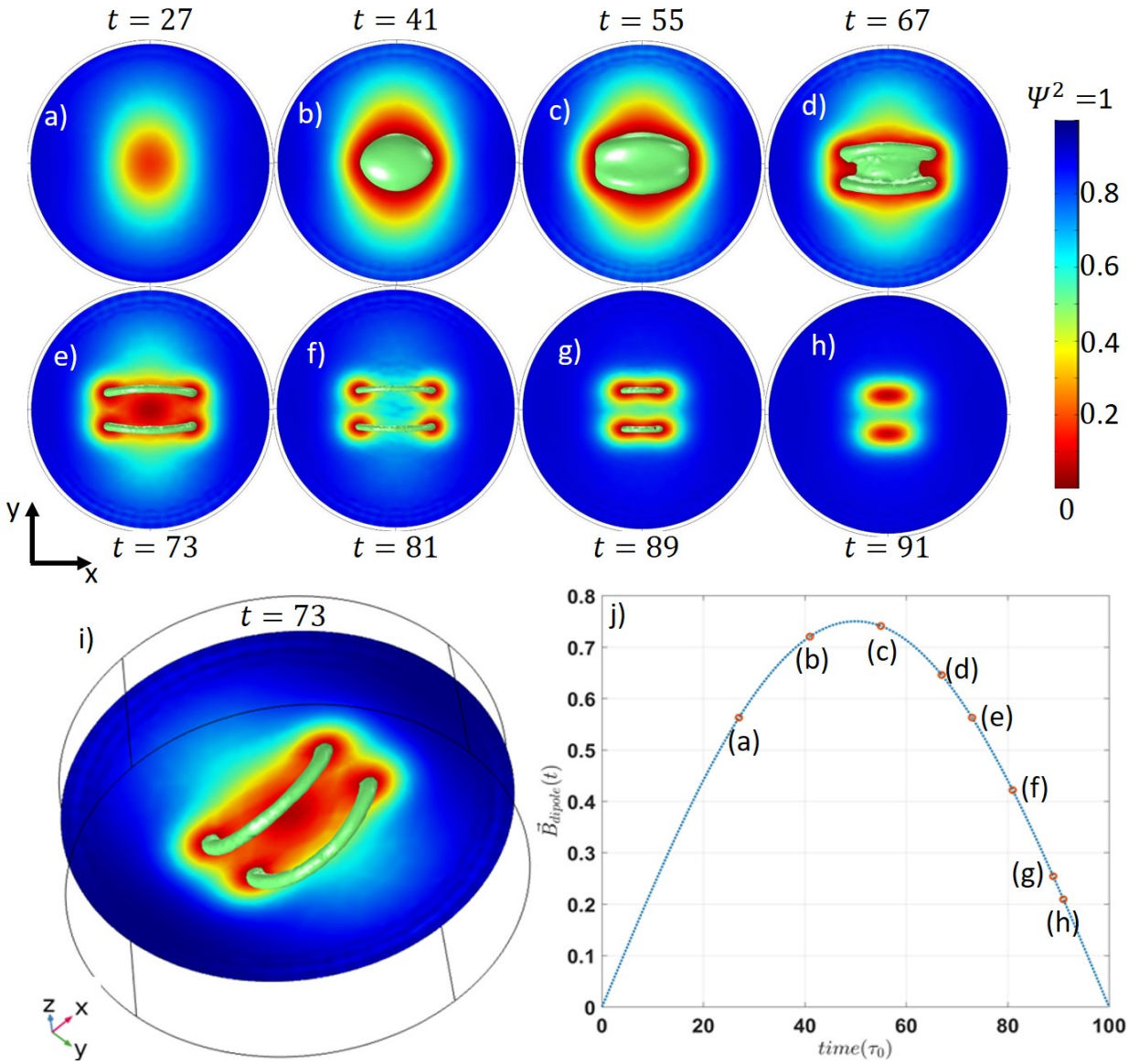

Figure 12: (Loking from inside the superconducting domain into the vacuum domain) a-h: Ψ^2 evaluated at the surface at different times for a Parallel Magnetic dipole above the Superconductor. $\vec{M}(t)$ is chosen such that $\vec{B}(t) = 0.75sin(\omega t)\hat{x}$. i: Same result as shown in figure 12.e) but from different angle. Green contours show the vortex semiloops. j: B_{dipole} at the surface vs time. Red circles correspond to snapshots a-h

The first simulation is done with $R = 12$, $H_{sc} = 6$, $H_{vac} = 3$, $\kappa = 1$, $\eta = 1.675$, $H_{dipole} = 8$, $\vec{B}_{dipole} = 0.75sin(\omega t)$,

$T = 0$ and $Period = 200$. The simulation was run for 3 periods to stabilize and the results shown in figure 12 are calculated during 4^{th} period. We see that as $\vec{B}(t)$ increases a normal state domain forms at the origin. Later as magnetic field direction is reversed the normal domain vanishes and vortex semi-loops emerge from it.

We can also cut a slice at $x = 0$ and see how vortices affect currents inside the superconductor (Figure 13).

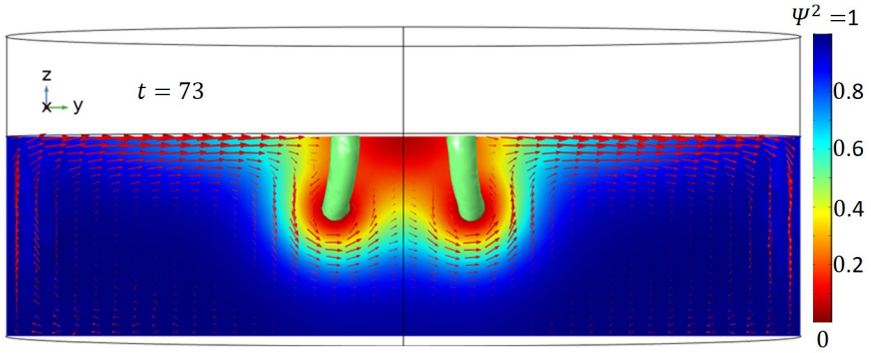

Figure 13: Ψ^2 and J_{surf} at t=73. Same result as shown in figure 12.e), y-z plane slice at x=0. Red arrows indicate the currents induced inside the superconducting domain.

3.2.2 Vortex Semi-loops as function magnetic field strength

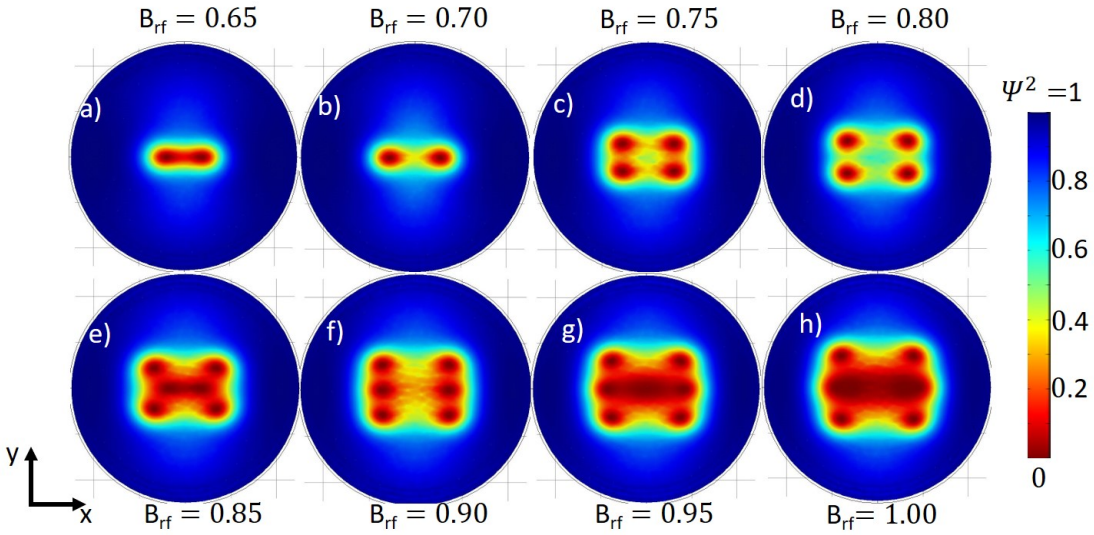

Figure 14: Ψ^2 at different rf field amplitudes for a Parallel Magnetic dipole above the Superconductor. $\vec{M}(t)$ is chosen such that $\vec{B}(t) = B_{rf} sin(\omega t)\hat{x}$. t=75 in all images.

Once we successfully modeled time evolution of vortex semi-loop at $B_{rf} = 0.75$ (shown in Figure 12), we redid the

same simulation for other values of B_{rf} (shown in Figure 14).

The most important parameter we can extract from this simulation is the magnetic field produced by currents induced inside the superconducting domain. This calculation is simplified due to the symmetric nature of the problem. At the location of the dipole, magnetic field is produced only in $\hat{x}$ direction.

Also, only $J_{\hat{y}}$ can produce magnetic field in x direction since the contribution from $J_{\hat{z}}$ will cancel out due to the symmetry.

The BiotSavart law dictates (normalized):

$$B_{sc} = \int_V dV \frac{\vec{J} \times \hat{r}}{r^2} = \int_V dV \frac{J_y H_{dipole}}{\left(x^2 + y^2 + (z - H^2_{dipole})\right)^{3/2}} \tag{36}$$

where B_{sc} is superconductor screening field and $\vec{r}$ is the vector from dV to dipole location.

Using Eq.(36) Magnetic field produced by the superconductor at the dipole location was calculated, and is shown in Fig. 15.:

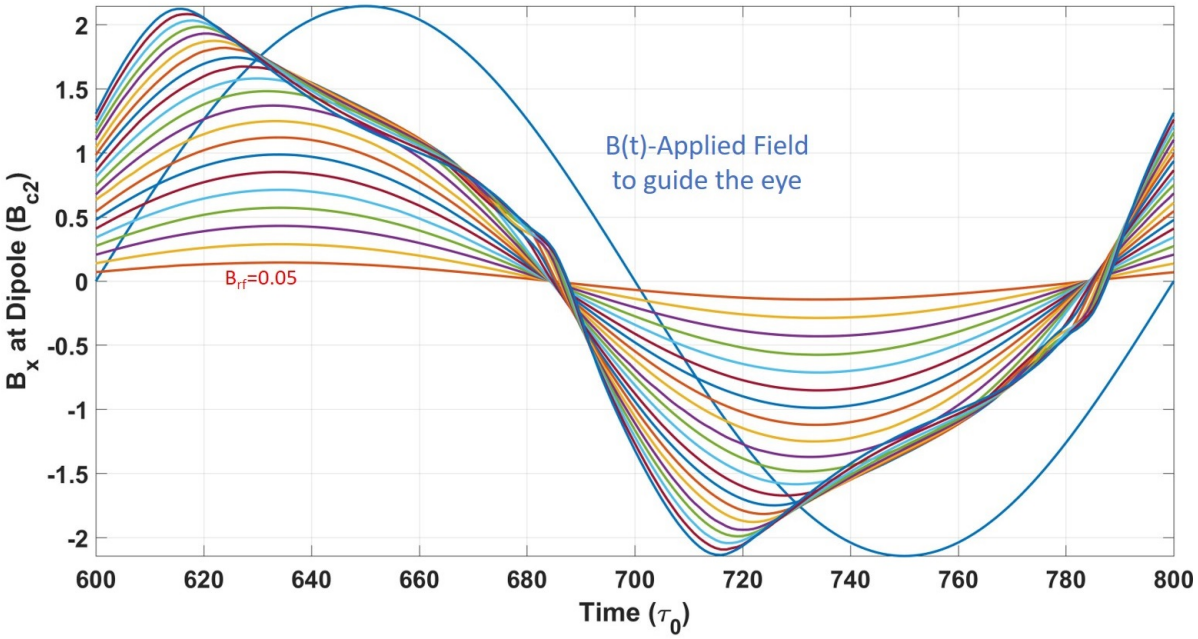

Figure 15: B_{sc} vs time at dipole location for $B_{rf} = [0.05 : 0.05 : 1.05]$

Figure 15 shows that at high enough B_{rf} values B_{sc} is not sinusoidal anymore. This is an indicates that this process should generate harmonic response. By taking the Fourier transformation of B_{sc} we can get harmonic response (Figure 16). The result is that we see monotonic increase of third harmonic response as a function of B_{rf}. In experiment we had seen periodic response as a function applied rf field amplitude. Thus, our simulation can't explain the data yet. The next step is to include defects.

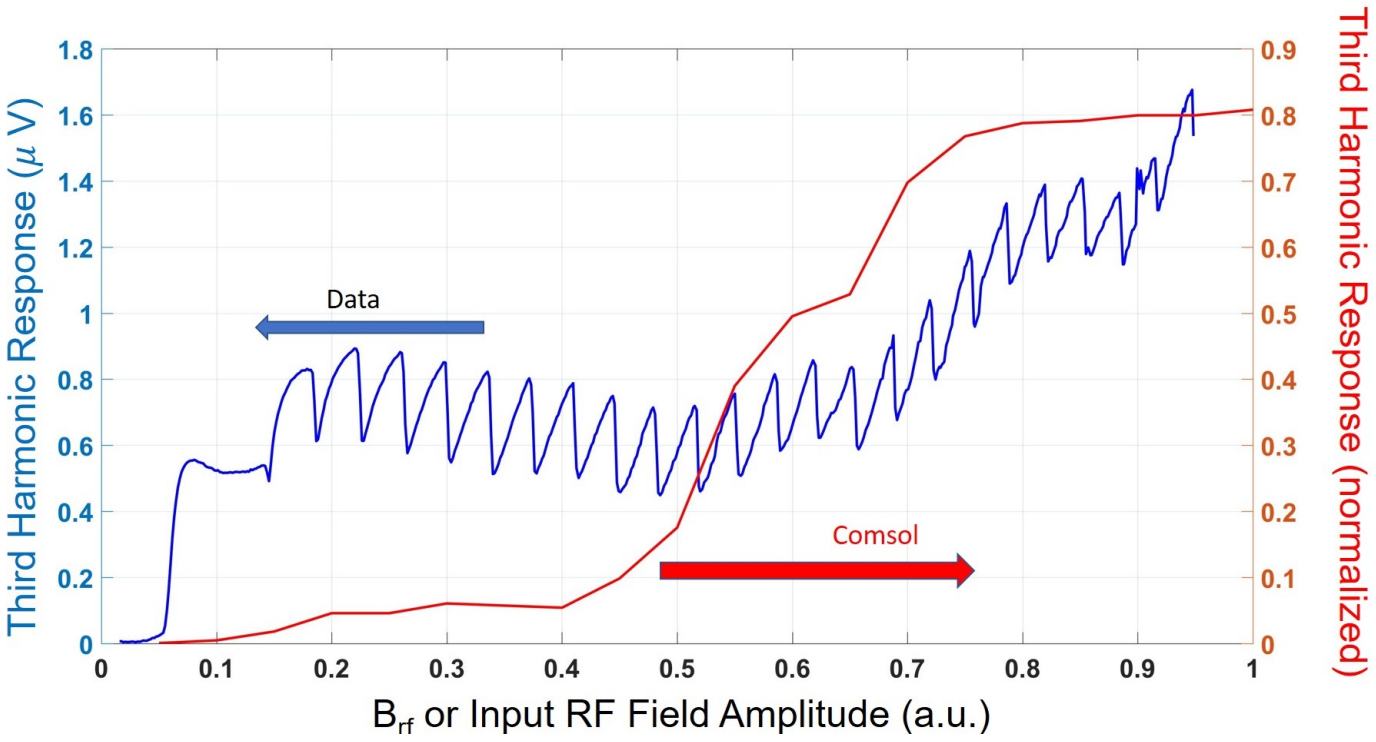

Figure 16: Left(Blue): Data from Bulk Nb sample measured via Near-Field MW Microscope (x-axes scaled). Right(Red): Third harmonic response measured at the location of the dipole as a function of peak B_{rf} value.

3.2.3 Usage of Defects

If we go back to equation 18, we see the usage of ϵ. Till now we were assigning $\epsilon(\vec{r}, Temperature) = 1 - \frac{Temperature}{T_c(\vec{r})}$ which correspond to pure superconductor with no defect. We can edit $\epsilon(\vec{r}, T)$ to add defects into the simulation.

The simplest defect can be defined by defining a domain with suppressed T_c. Lets redefine T_c as:

$$T_c(\vec{r}) = T_{cBulk} - (T_{cBulk} - T_{cDefect})\, e^{-\frac{(x-x_d)^2}{2\sigma_x} - \frac{(y-y_d)^2}{2\sigma_y} - \frac{(z-z_d)^2}{2\sigma_z}} \tag{37}$$

where x_d, y_d, z_d are the coordinates of the defect and $\sigma_x, \sigma_y, \sigma_z$ are the standard deviations in 3 coordinate axes. This defects can be used as pinning sites to study the interaction between vortex semiloops and pinning sites.

The example shown in figure 17 is computed with $R = 30$, $H_{sc} = 15$, $H_{vac} = 10$, $\kappa = 1$, $\eta = 1.675$, $H_{dipole} = 12$, $\vec{B}_{dipole} = 0.3sin(\omega t)$, $T = 8.5K$ and $Period = 200$. A domain with $\sigma_x = \sigma_y = \sigma_z = \sqrt{2}$ and $T_{cDefect} = 2K$ is located at $\vec{r} = 10\hat{x} + 20\hat{y} - 8\hat{z}$ to represent a localized defect. The simulation was run for 3 periods to stabilize and the results are extracted during 4^{th} period. We see that as $\vec{B}(t)$ increases a normal state domain forms at the origin. Later as magnetic field direction is reversed the normal domain vanishes and vortex semi-loops emerge from it, similar to what we have seen in figure 12.

Using equation 36 and taking its fourier transformation we can get harmonic response produced by interaction between vortex semiloop and localized defect. This harmonic response is shown in figure 18. The result is that as a function of B_{rf} third harmonic response rises monotonically, reaches a peak and decreases monotonically. It is very

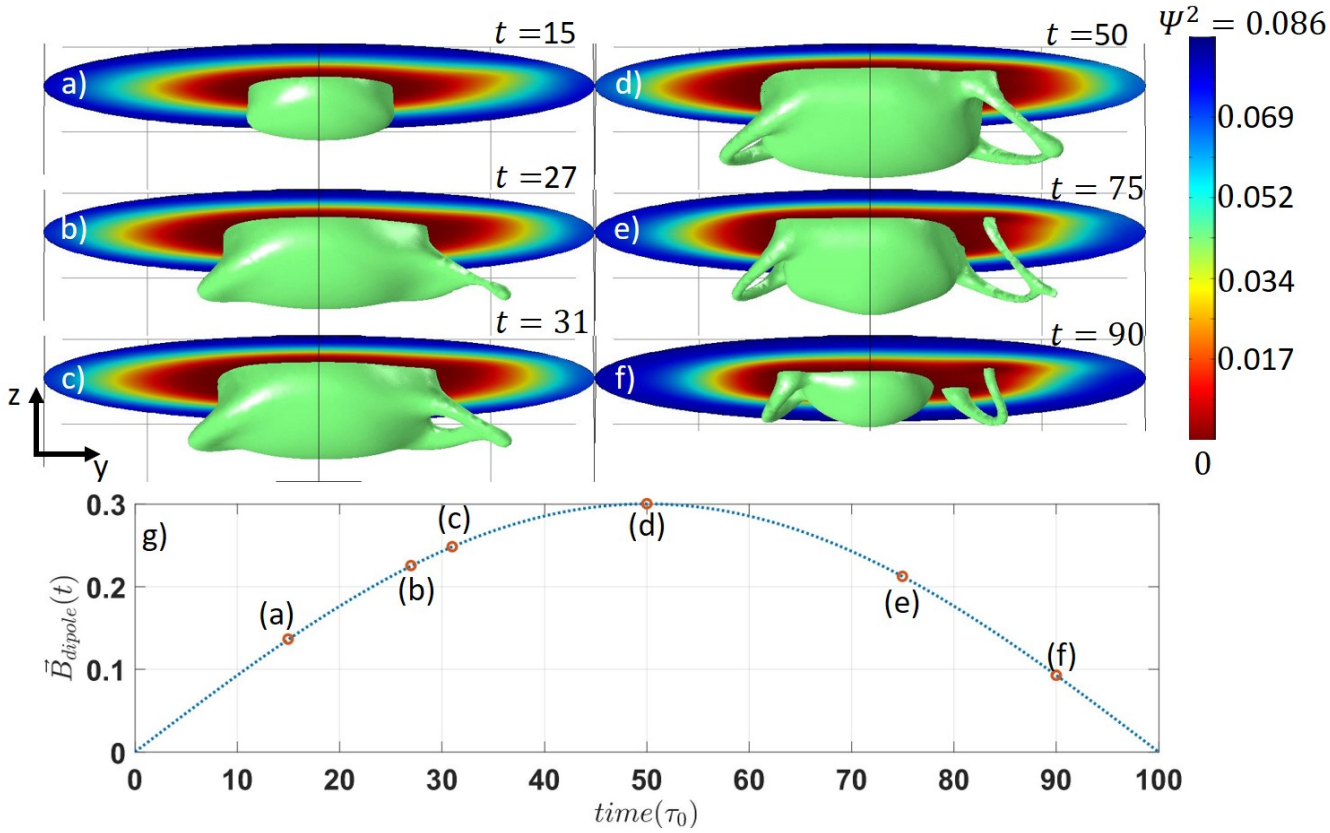

Figure 17: (Loking from +x towards the origin) a-f: Ψ^2 contours show the vortex semiloops at different times for a Parallel Magnetic dipole above the Superconductor. $\vec{M}(t)$ is chosen such that $\vec{B}(t) = 0.3sin(\omega t)\hat{x}$. g: B_{dipole} at the surface vs time. Red circles correspond to snapshots a-f

different from result obtained without a defect, but still not close enough to explain our experimental data (see figure 16). Moreover, when the same simulation was repeated without a defect, same behavior was observed meaning that this result is not due to the defect but due to the higher temperatures used compared to zero temperature results shown in figures 12 and 14.

3.2.4 The effect of η value

In section 1.5 we defined η as

$$\eta = \frac{3}{\mu_0 \kappa^2 \sigma_n v_F l}$$

We can draw parallel with the fluid mechanics to understand the physical nature of η. If the superconductor is the fluid and the vortex is a particle or a local feature moving the fluid, η would represent viscosity of that fluid. Materials

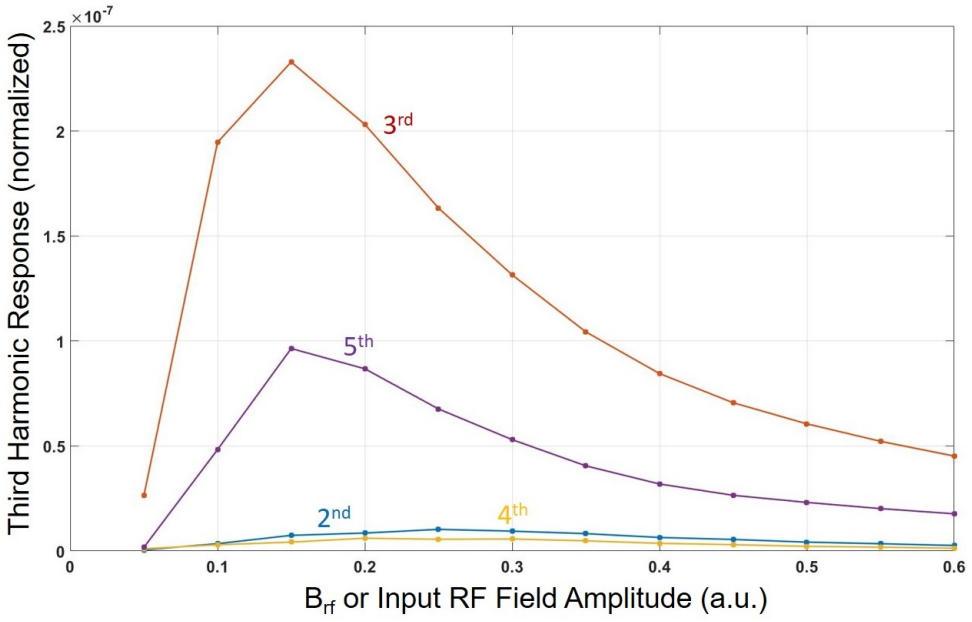

Figure 18: Third harmonic response measured at the location of the dipole as a function of peak B_{rf} value.

in clean limit will have bigger l-mean free path thus lower η-"viscosity", on other hand materials with higher density of impurities (dirty limit) will have lower mean free path, thus higher "viscosity".

In order to observe this effect we simulated same scenario as in section 3.2.3 for different values of η but without any defect. The results are shown in figure 19. We see that for lower values of η the vortex semiloops penetrate further as expected. So the lower η the further features generated at surface will reach.

We also can see the change in the size of the normal state domain formed at origin. For low η values, formation of vortex semiloops provides the needed relaxation and we have relatively small sized normal state domain. For high η values, there is not enough time for the normal state domain to penetrate inside the bulk of the superconductor. When η value is between this 2 limiting cases, the normal state domain size is very big, because there is enough time for it to penetrate into the bulk, but there isn't enough time for vortex semiloops to form and emerge from this normal state domain.

We also note that the vortex semiloops and normal state domain are reaching the boundaries of simulation. Although it might lead to nonphysical results, we believe the general dynamics is the same and for qualitative argument those edge effects can be neglected.

3.3 Vortex Semiloops in SRF Cavity

In section 3.2 we studied the dynamics of vortex semiloops creatded by a point magnetic dipole. In this section we will try to address more general case, a uniform magnetic field above the superconductor in the presence of defects. We will study DC, RF and DC+RF cases.

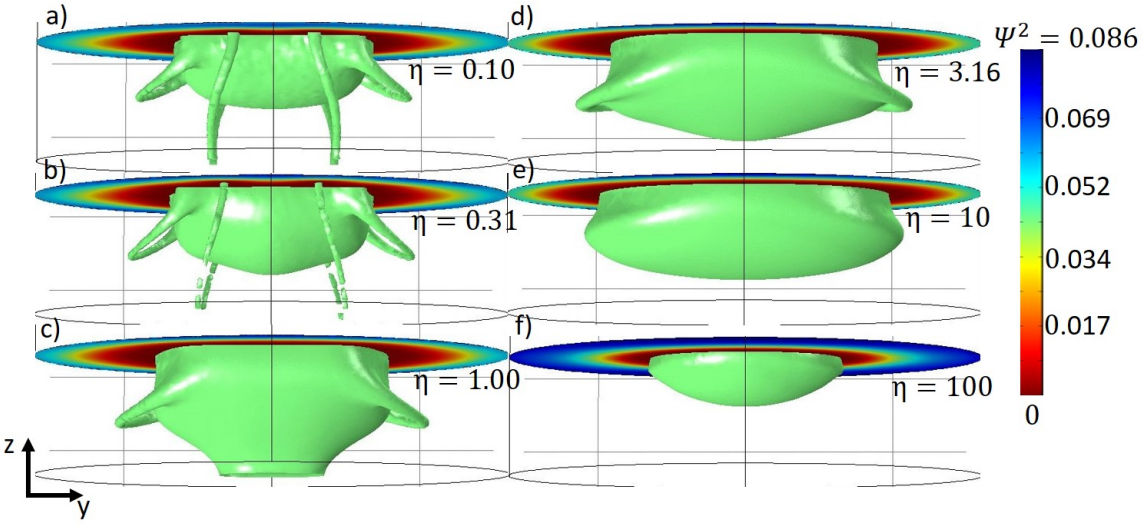

Figure 19: (Loking from +x towards the origin) Ψ^2 contours show the vortex semiloops for a Parallel Magnetic dipole above the Superconductor at t=150 which corresponds to peak value of $B_{dipole}(t) = 0.4$. a: $\eta = 0.10$, b: $\eta = 0.31$, c: $\eta = 1.00$, d: $\eta = 3.16$, e: $\eta = 10$, f: $\eta = 100$.

3.3.1 Modeling Uniform Magnetic Field

As always the first task is to model a uniform magnetic field on the surface of an SRF cavity. In order to have truly uniform field, the boundary between superconductor and air/vacuum should be simulated as an infinite plane. Same steps as in sections 2.3.2 were used with slightly modified boundary conditions.

The dimain used for simulation is a simple block as shown in figure 20. There is a similar vacuum domain on top of the superconducting domain which is not shown in figure, but was discussed before at length in section 2.3.2. The boundary conditions are as follows:

For the top boundary of the superconducting domain (labeled 3 in figure 20) is the only physical boundary between the superconductor and vacuum. All other boundaries are mathematical and do not exist in the physical picture because the geometry is infinite in $\pm\hat{x}$, $\pm\hat{y}$ and $-\hat{z}$. For this top boundary:

$$\vec{\nabla}\Psi \cdot \hat{n} = 0 \quad or\ equally \quad \vec{\nabla}\Gamma \cdot \hat{n} = 0$$
$$and\ \vec{A} \cdot \hat{n} = 0 \quad or\ equally \quad \vec{u} \cdot \hat{n} = -\vec{A}_{ext} \cdot \hat{n}$$

For the boundary at the bottom which should extend to infinity:

$$\vec{\nabla}\Psi \cdot \hat{n} = 0 \quad or\ equally \quad \vec{\nabla}\Gamma \cdot \hat{n} = 0$$
$$and\ \vec{A} = 0 \quad or\ equally \quad \vec{u} = -\vec{A}_{ext}$$
$$and\ |\Psi|^2 = 1 - \frac{T}{T_c}$$

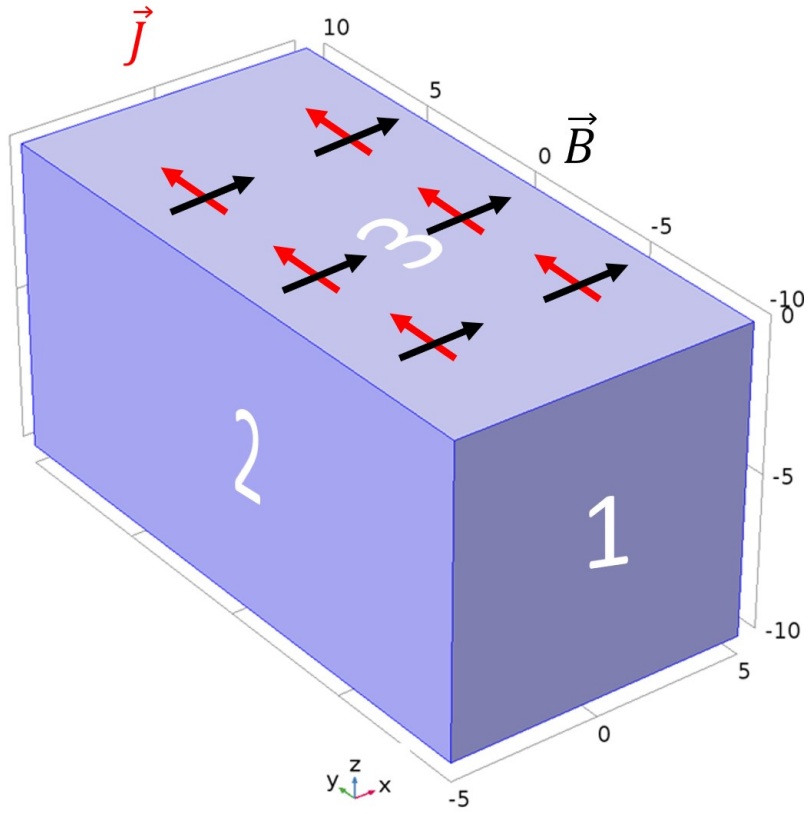

Figure 20: The superconducting domain used. $\vec{B}$ and $\vec{J}$ show the directions of applied magnetic field and resulting screening current respectively

.

where T is the Temperature and T˙c is the characteristic critical temperature of the superconductor. Here the assumption is that this boundary is sufficiently deep inside the superconductor that any externally applied field is screened before it reaches here.

For the boundaries at $\pm\hat{x}$ and $\pm\hat{y}$ (1,2 and opposite sides in figure 20):

$$\vec{\nabla}\Psi \cdot \hat{n} = 0 \quad or\ equally \quad \vec{\nabla}\Gamma \cdot \hat{n} = 0$$
$$and\ \vec{A_x} = \vec{A_z} = 0 \quad or\ equally \quad \vec{u}_x = -\vec{A}_{x_{ext}} \quad and\ \vec{u}_z = -\vec{A}_{z_{ext}}$$

Here $\vec{A_x}$ indicates $\hat{x}$ component of $\vec{A}$. We also assighned periodic boundary conditions (periodic both in $\hat{x}$ and $\hat{y}$) on Ψ and $\vec{A}$. For this boundaries there is no condition for $\vec{A_y}$ since the uniform current running in $\hat{y}$ direction will contribute to $\vec{A_y}$.

Again it is assumed that the simulation domain is big enough and any contributions due to defects and local semiloop vortices will not reach this boundaries.

In order to model the uniform magnetic field in x, external vector magnetic potential was set to: (see Eq. 35 for definition)

$$\vec{A}_{ext} = -B_x z \hat{y}$$

In order to test the model the simplest scenario was tested. A uniform but weak magnetic field was applied and the surface current was plotted as a function of the depth inside the superconductor. The results are shown in figure 21. Here we didn't include any defects and the temperature dependence of ϵ is assigned as follows:

$$\epsilon(\vec{r}, T) = 1 - \frac{T}{T_c}$$

$$\lambda(T) = \frac{\lambda_0}{\sqrt{1 - \frac{T}{Tc}}} \tag{38}$$

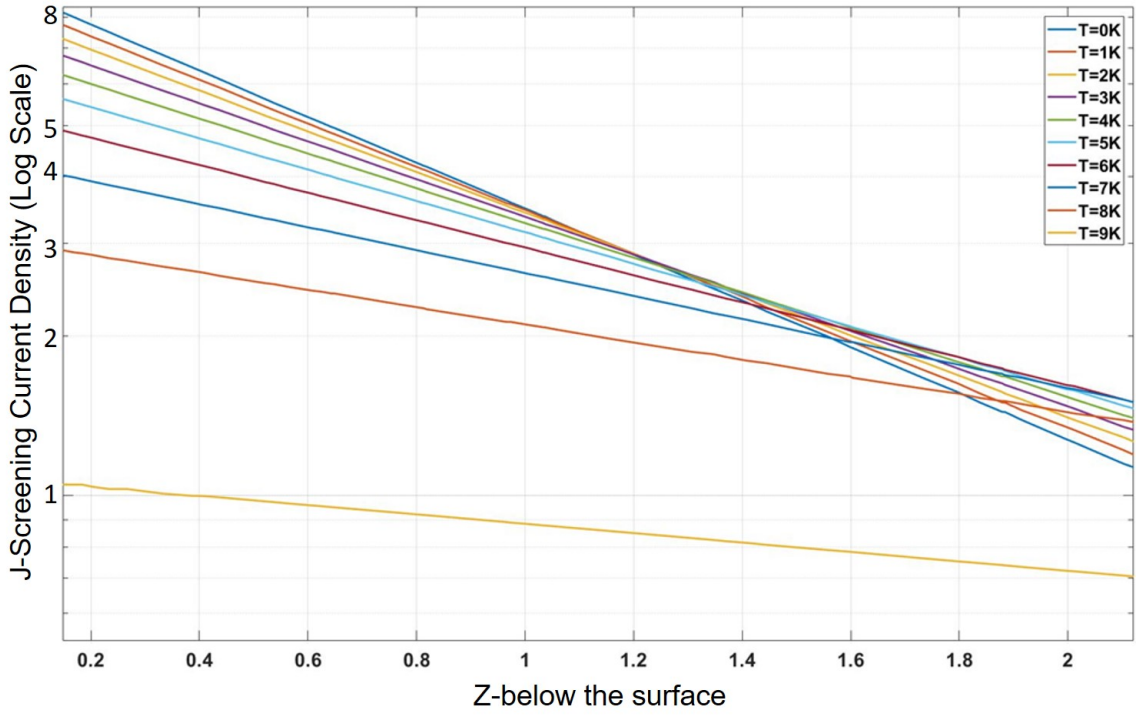

Figure 21: The density of the screening current as a function of depth below the surface. $T_c = 9.3K$.

.

We clearly see that the currents are decaying exponentially and the characteristic decay length depends on temperature. This outcome was already expected from London Equations. The slope of this lines gives the penetration depth, which is plotted as a function of temperature in figure 22. Since penetration depth is inversely proportional to $|\Psi|^2$ we can write an equation defining the temperature dependence of penetration depth:

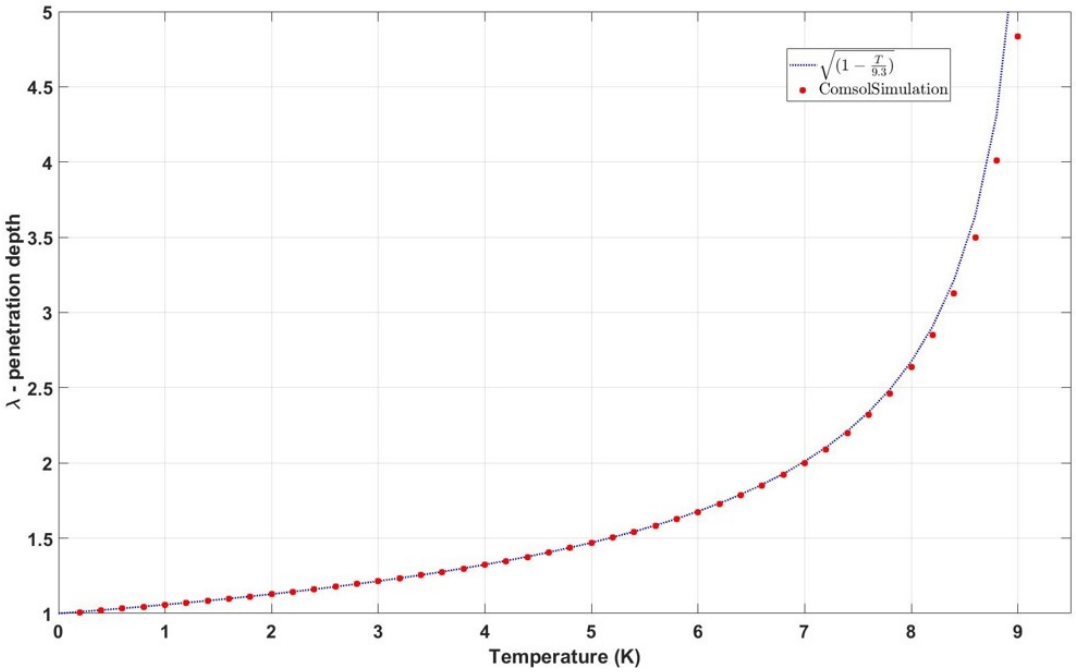

Figure 22: Penetration depth versus Temperature

.

3.3.2 Vortex Semiloop

Once we tested and verified our model we first did simulation for a rectangular prism shaped superconductor domain with size of 80 x 60 x 20 and a similarly shaped vacuum domain with height of 10 on top of the superconducting domain. Here $\kappa = 1$, $\eta = 0.1$, $\vec{B}(t) = 0.75sin(\omega t)\hat{x}$, $T = 2K$ and $Period = 1000$. The simulation was run for 3 periods to stabilize and the results shown in figure 23 are calculated during 4^{th} period.

A defect was introduced at the origin in the same fashion as described in section 3.2.3. The parameters for the defect were chosen as follows $x_d = y_d = 0$, $z_d = -1$ are the coordinates of the defect and $\sigma_x = 6$ and $\sigma_y = \sigma_z = 1$ are its standard deviation. The defect has a $T_{cDefect} = 1K$.

We see that as $\vec{B}(t)$ increases a vortex semiloop enters the superconductor and moves deeper into the bulk. After $t = 500$ the direction of the magnetic field changes and we see an antivortex entering the superconductor (Fig23.c). At $t = 725$ Vortex and Antivortex semiloops meet each other (Fig23.d). At $t = 728$ we see how they form 2 new vortex semiloops (Fig23.e) which quickly collapse (Fig23.f). This the first numerical simulation of the model described in [13].

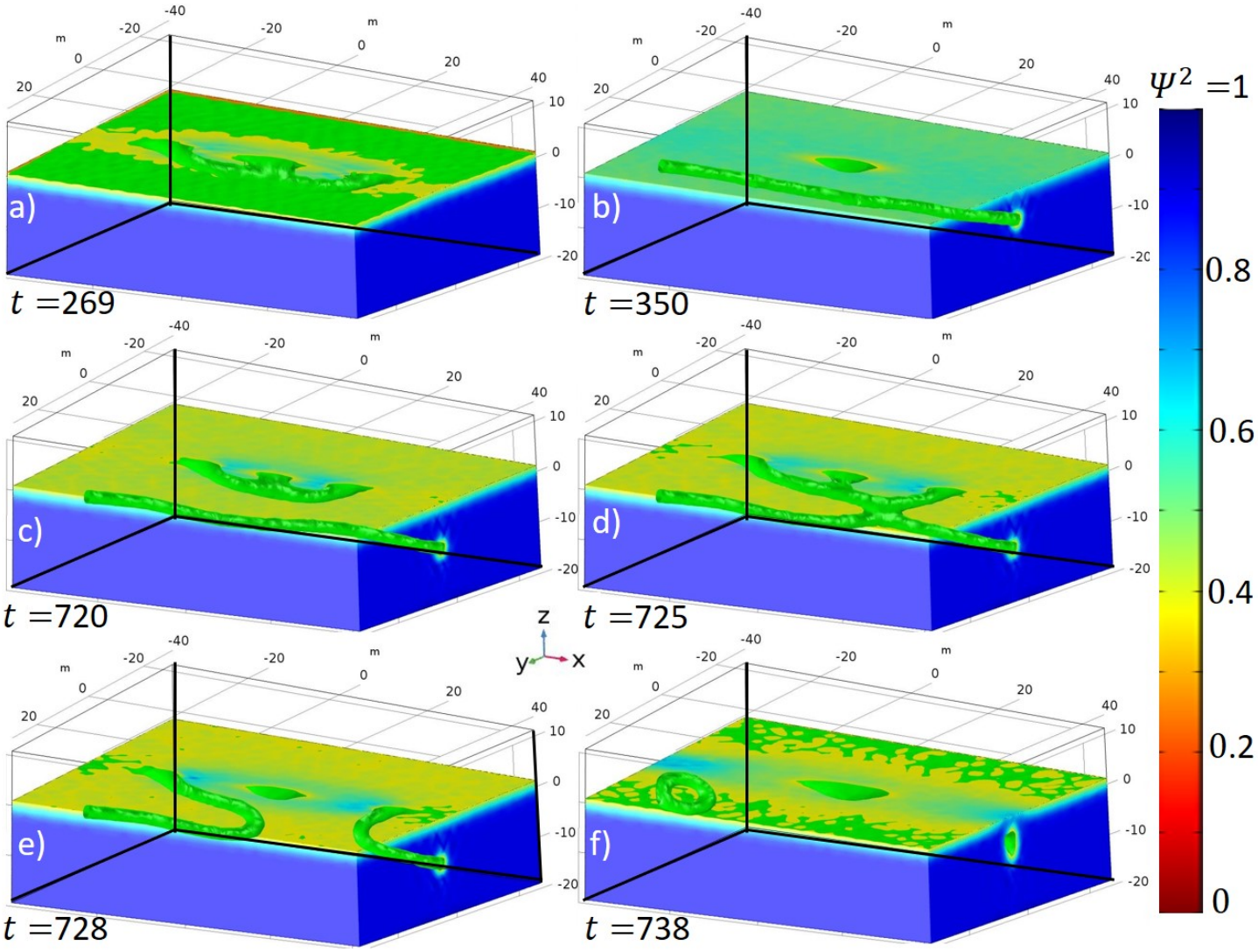

Figure 23: (Loking from inside the superconducting domain into the vacuum domain, 3 thick black edges are the closest edges to the camera) a-h: Ψ^2 evaluated at different times for a uniform magnetic field applied along $\hat{(x)}$ axis. $\vec{B}(t) = 0.75sin(\omega t)\hat{x}$.

.

References

[1] Henley, Christopher. *Ginzburg-Landau theory lecture.* `http://www.lassp.cornell.edu/clh//BT-GL/6.1.pdf`

[2] Duxbury, Phillip M. *Ginzburg-Landau theory, modeling of dynamics and scaling in complex systems.* http://web.pa.msu.edu/people/duxbury/courses/phy831/LectureNotesAndProblemsPart4.pdf

[3] L. P. Gor'kov. *Microscopic derivation of the Ginzburg-Landau Equations in the Theory of Superconductivity.* J. Exptl. Theoret. Phys. (U.S.S.R.) 36, 1918-1923 (June,1959).

[4] Gropp, W.D., Kaper, H.G., Leaf, G.K., Levine, D.M., Palumbo, M., Vinokur, V.M. *Numerical simulations of vortex dynamics in Type-II superconductors.* J. Comput. Phys. 123, 254266 (1996).

[5] I.A.Sadovskyya, A.E.Kosheleva, C.L.Phillipsb, D.A.Karpeyevc, A.Glatza. *Stable large-scale solver for Ginzburg-Landau equations for superconductors.* Journal of Computational Physics,Volume 294, (August,2015).

[6] L.P. Gorkov, G.M. liashberg. *Generalization of the GinzburgLandau equations for non-stationary problems in the case of alloys with paramagnetic impurities.* Sov. Phys. JETP 27 (1968) 328.

[7] M Cyrot. *Ginzburg-Landau theory for superconductors.* Repts. Prog. Phys. 36, 103 (1973).

[8] I. S. Aranson, N. B. Kopnin, and V. M. Vinokur. *Dynamics of vortex nucleation by rapid thermal quench.* Physical Review B, vol 63, 184501, (2001).

[9] T.S. Alstrom, M. P. Sorensen, N. F. Pedersen, S. Madsen. *Magnetic Flux Lines in Complex Geometry Type-II Superconductors Studied by the Time Dependent Ginzburg-Landau Equation.* Acta Appl Math (2011) 115: 63. https://doi.org/10.1007/s10440-010-9580-8

[10] Ernesto A. Matute. *On the superconducting sphere in an external magnetic field.* American Journal of Physics 67, 786 (1999). https://doi.org/10.1119/1.19126

[11] M. V. Milosevic, S. V. Yampolskii, and F. M. Peeters. *Magnetic pinning of vortices in a superconducting film: The antivortex magnetic dipole interaction energy in the London approximation.* Phys. Rev. B 66, 174519, (2002).

[12] A. S. Melnikov, Yu. N. Nozdrin, I. D. Tokman, and P. P. Vysheslavtsev. *Experimental investigation of a local mixed state induced by a small ferromagnetic particle in Y-Ba-Cu-O films: Extremely low energy barrier for formation of vortex-antivortex pairs.* Phys Rev B Vol 58, 17 (1998).

[13] A. Gurevich, G. Ciovati. *Dynamics of vortex penetration, jumpwise instabilities, and nonlinear surface resistance of type-II superconductors in strong rf fields.* Phys. Rev. B 77, 104501, (2008).

[14] Tamin Tai. *Measuring electromagnetic properties of superconductors in high and localized rf magnetic field.* PhD Thesis (2012). https://drum.lib.umd.edu/handle/1903/14668

[15] Arup Ratan Jana, Abhay Kumar, Vinit Kumar, Sindhunil Barman Roy. *Influence of material parameters on the performance of niobium based superconducting RF cavities.* arXiv:1703.07985 [physics.acc-ph].

[16] http://hyperphysics.phy-astr.gsu.edu/hbase/Solids/chrlen.html

[17] Pavel Lipavsky, Jan Kolcek, Klaus Morawetz, Ernst Helmut Brandt, Tzong-Jer Yang. *Bernoulli Potential in Superconductors: How the Electrostatic Field Helps to Understand Superconductivity.* Volume 733 of Lecture Notes in Physics.

[18] http://hyperphysics.phy-astr.gsu.edu/hbase/Tables/fermi.html